iScience

CellPress
OPEN ACCESS

Article

Streptococcus pneumoniae promotes lung cancer development and progression

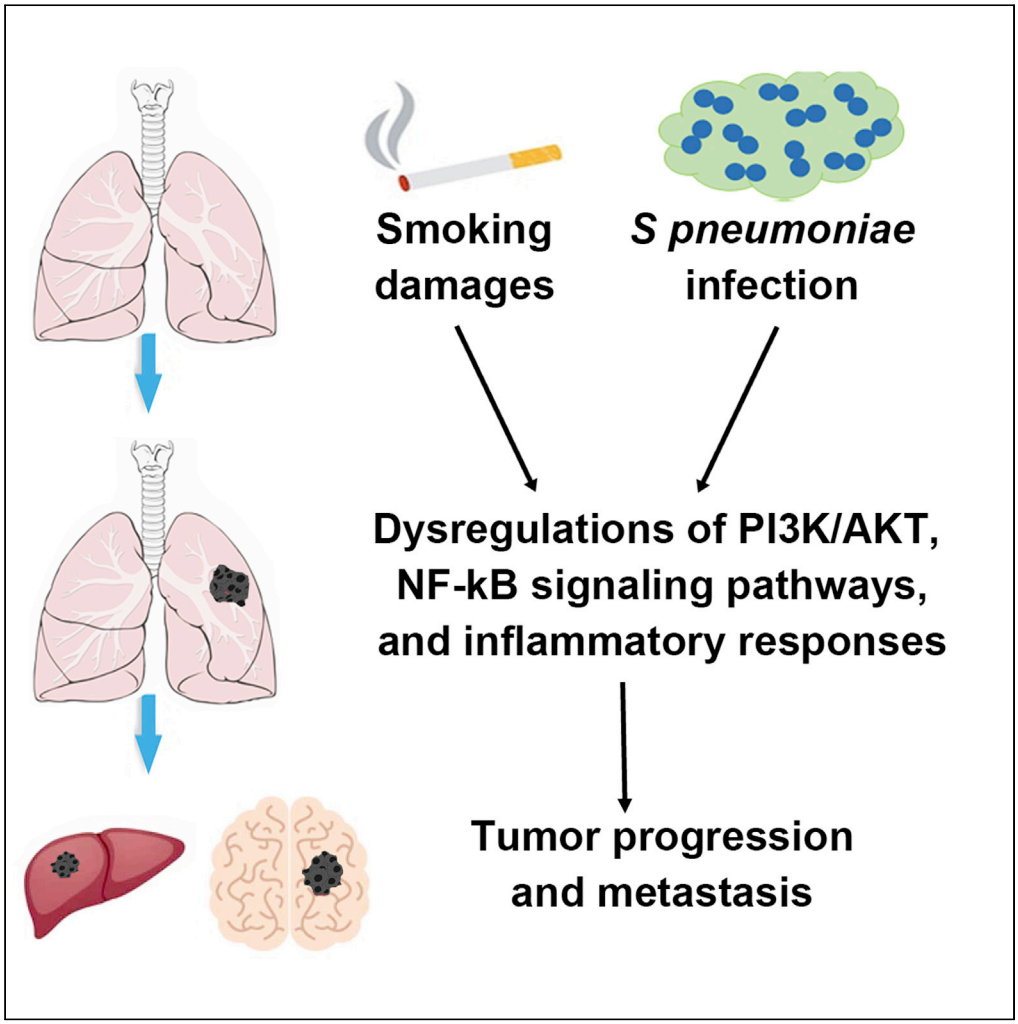

Ning Li, Huifen Zhou, Van K. Holden, ..., Nevins W. Todd, Sanford A. Stass, Feng Jiang

fjiang@som.umaryland.edu

Highlights

S. pneumoniae (SP) attaches to cells via binding to platelet-activating factor receptor

Lung cancer cells with *SP* form larger tumors in mice compared to untreated cells

Overabundance of *SP* is associated with the survival of lung cancer patients

SP may provide a microbial target for diagnosis and treatment of lung cancer

Li et al., iScience *26*, 105923
February 17, 2023
https://doi.org/10.1016/j.isci.2022.105923

iScience

CellPress
OPEN ACCESS

Article

Streptococcus pneumoniae promotes lung cancer development and progression

Ning Li,[1,2] Huifen Zhou,[1] Van K. Holden,[2] Janaki Deepak,[2] Pushpa Dhilipkannah,[1] Nevins W. Todd,[2] Sanford A. Stass,[1] and Feng Jiang[1,3,*]

SUMMARY

***Streptococcus pneumoniae (SP)* is associated with lung cancer, yet its role in the tumorigenesis remains uncertain. Herein we find that *SP* attaches to lung cancer cells via binding pneumococcal surface protein C (PspC) to platelet-activating factor receptor (PAFR). Interaction between PspC and PAFR stimulates cell proliferation and activates PI3K/AKT and nuclear factor kB (NF-kB) signaling pathways, which trigger a pro-inflammatory response. Lung cancer cells infected with *SP* form larger tumors in BALB/C mice compared to untreated cells. Mice treated with tobacco carcinogen and *SP* develop more lung tumors and had shorter survival period than mice treated with the carcinogen alone. Mutating PspC or PAFR abolishes tumor-promoting effects of *SP*. Overabundance of *SP* is associated with the survival. *SP* may play a driving role in lung tumorigenesis by activating PI3K/AKT and NF-kB pathways via binding PspC to PAFR and provide a microbial target for diagnosis and treatment of the disease.**

INTRODUCTION

Lung cancer ranks among the most frequent cancers in the world and is the leading cause of cancer-related deaths in men and women.[1] Over 85% of lung cancers are non-small cell lung cancer (NSCLC), which mainly consists of adenocarcinoma (AC) and squamous cell carcinoma (SCC). The underlying mechanisms for the development and progression of NSCLC have not been completely elucidated. The microbiome, defined as the collection of microbiota and their genes, plays an important role in health and diseases.[2] Microbiota aberrations are attributed to tumorigenesis through different mechanisms, such as damage of the local immune barrier, production of bacterial toxins that alter host genome stability, and release of cancer-promoting microbial metabolites.[3] Furthermore, intratumoral microbes may directly affect the growth and metastatic spread of tumor cells.[2] Infection of *Human Papilloma virus, Epstein-Barr virus, Helicobacter pylori*, *Escherichia coli*, and *Fusobacterium nucleatum* can cause human malignancies, including cervical, nasopharyngeal, and gastrointestinal cancers.[2]

As the second microbiome habitat behind the alimentary canal in the human body, the respiratory tract harbors abundant microbiota, containing more than 500 different species of bacteria.[4–7] Patients with lung cancer have lower microbial diversity and altered abundances of particular bacteria compared with cancer-free individuals.[8] 16S rRNA gene sequencing-based studies have identified a set of bacterial genera with either higher or lower abundances in lung tumors vs. normal lung tissues.[9–16] Greathouse et al. showed that *Acidovorax* was abundant in TP53 mutation-positive lung SCC specimens.[17] Tsay et al. found that airway microbiota affected the progression of NSCLC.[14,16]

As early as 1868, William Busch reported spontaneous tumor regressions in patients with *Streptococcal* infections.[18] Since then, mounting evidence suggests that *Streptococcus pneumoniae* (*SP*) is associated with human tumors, particularly lung cancer.[14,19,20] However, it remains uncertain whether *SP* is a causative pathogen in carcinogenesis or only an opportunistic pathogen or simply commensal bacteria associated with the microenvironment. Furthermore, although numerous bacteria have been suggested to cause human tumors, none has been characterized as a major player in lung tumorgenicity. Here we investigate the role of *SP* in the tumorigenesis of NSCLC and provide the evidence for oncogenic function of microbiota dysbiosis in the development and progression of lung cancer.

[1]Department of Pathology, University of Maryland School of Medicine, Baltimore, MD, USA

[2]Department of Medicine, University of Maryland School of Medicine, Baltimore, MD, USA

[3]Lead contact

*Correspondence: fjiang@som.umaryland.edu

https://doi.org/10.1016/j.isci.2022.105923

RESULTS

SP attaches to and invades lung cancer cells via binding pneumococcal surface protein C (PspC) to platelet-activating factor receptor (PAFR)

Adhesion and invasion of bacteria to host cells are essential to cause diseases.[21] PAFR is a key adhesion receptor for *SP* in airway cells and significantly upregulated in NSCLC tissue specimens.[22–24] To test the role of PAFR in the attachment and invasion of *SP* to lung cancer cells, we first analyzed expression of PAFR in NSCLC cell lines (H226, H460, and H1299) and a normal lung epithelial cell line (BEAS-2B). H460 and H1299 cell lines had a higher level of PAFR expression compared with H226 cells and BEAS-2B cells (Figure 1A). We then explored the capability of *SP* to attach to and invade the cells. *SP* had a significantly higher level of adhesion and invasion to H460 and H1299 cancer cells compared with H226 cells and BEAS-2B cells (Figure 1B). Fluorescence *in situ* hybridization (FISH) showed that *SP* was enriched in H460 and H1299 cancer cells compared with H226 cells and BEAS-2B cells (Figure 1C). Furthermore, *SP* had a higher level of adhesion and invasion to H460 and H1299 cancer cells compared with *Enterococcus faecalis (E. faecalis)* and heat-killed *SP* (Figure 1B). Therefore, *SP* could selectively attach to and invade the lung cancer cells that had high PAFR activation.

Pneumococcal surface proteins A and C (PspA and PspC) are among the major factors that interact with respiratory epithelial cells.[6,21,25] Particularly, PspC can specifically bind to PAFR on host cells.[6,21,25] Thus, we tested the role of the surface proteins' binding to PAFR in attachment and invasion of *SP*. PspC-deficient mutant *SP* lost adhesion and invasion to H460 and H1299 cancer cells, whereas PspA-deficient mutant *SP* maintained the activities (Figure 1B). Furthermore, downregulation of PAFR by small interfering RNA (siRNA) in H460 and H1299 cells significantly inhibited attachment and invasion of *SP* (Figure 1D). To further inspect whether adhesion and invasion of *SP* to lung cancer cells is dependent on the binding, H460 and H1299 cells were treated with WEB2086, a PAFR antagonist, followed by *SP* infection. WEB2086 could suppress adhesion and invasion of *SP* to the cells in a dose-dependent manner (Figure 1E). In addition, enforced expression of PAFR in H226 cells increased attachment and invasion of wild-type *SP* and PspA-deficient mutant *SP*, not PspC-deficient mutant *SP* (Figure 1F). Taken together, adhesion and invasion of *SP* to cancer cells require binding of PspC to PAFR.

SP promotes the tumorigenicity of lung cancer by integrating PspC and PAFR

Binding of *SP* to host cells can dysregulate PAFR recycling pathway, leading to the initiation and development of diseases.[6,21] We first determined if *SP* infection could promote *in vitro* tumorgenicity of cancer cells. *SP* stimulated cell proliferation and migration of PAFR-expressing cells, H460 and H1299 cells (All <0.01) (Figures 2A and 2B). However, *E. faecalis* or heat-killed *SP* had no stimulatory effect in all NSCLC cells and BEAS-2B cells (Figures 2A and 2B). We further depleted PAFR in H1299 and H460 using PAFR-siRNA and then incubated the cells with *SP* (Figure 2C). The depletion of PAFR in H460 and H1299 cells significantly reduced the effect of *SP* on cell proliferation (Figure 2D). The depletion of PAFR in H460 and H1299 cancer cells inhibited the effect of *SP* on cell migration (Figure 2E). Furthermore, WEB2086, the PAFR antagonist, repressed the tumor-promoting effects of *SP* on the cells (Figures 2F and 2G). In addition, enforced activation of PAFR in H266 cancer cells increased the *SP*-induced tumorigenicity (Figures 2H and 2I). Therefore, *SP* infection could promote malignancy in NSCLC cells in a PAFR-dependent manner.

To determine if the integration of PspC and PAFR is essential for the tumor-promoting effects of *SP*, we treated cancer cells with wild-type, PspC- or PspA-deficient mutant *SPs*, respectively. The PAFR-expressing cells (H226 and H1299) infected with wild-type strain had higher cell proliferation and migration compared with the cells treated with PspC-deficient mutant *SP* (Figures 2A and 2B). Furthermore, H460 and H1299 cells infected with PspA-deficient mutant *SP* reserved the tumor-promoting effects of *SP* (Figures 2A and 2B). However, H226 cells infected with all wild-type and mutant *SPs* did not display elevated cell proliferation and migration (Figures 2A and 2B). Altogether, *SP* promotes lung tumorigenesis via integrating PspC and PAFR.

SP infection contributes to lung tumorigenesis by stimulating phosphatidylinositol 3-kinase (PI3K)/protein kinase B (AKT) and NF-kB signaling pathways

PAFR is a direct regulator of PI3K/AKT and nuclear factor kB (NF-kB) signaling pathways whose hyperactivations play essential roles in tumor development and progression.[14,26–30] We therefore evaluated expression of key molecular signatures of the pathways in cancer cells incubated with or without *SP*. *SP* effectively activated PI3K, AKT,

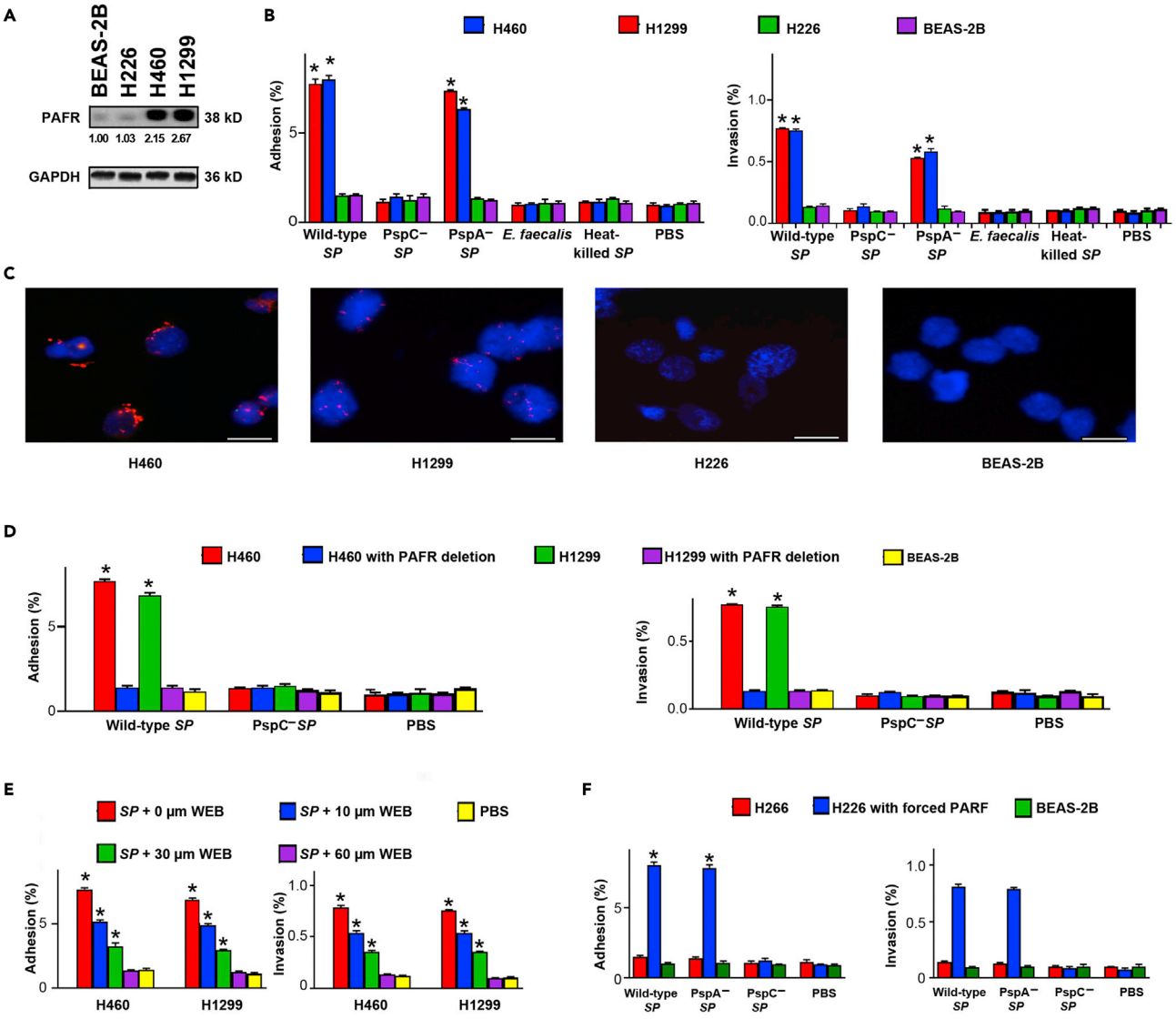

Figure 1. *SP* attaches to and invades lung cancer cells via binding PspC to PAFR

(A) PAFR expression was determined in cancer cell lines (H226, H460, and H1299) and a normal lung epithelial cell line (BEAS-2B) by Western blot. GAPDH was used as the loading control. Band intensity was determined by using ImageJ, and the ratio of each band was normalized to the corresponding GAPDH and shown below each band. H460 and H1299 cells had a higher level of PAFR expression compared with H226 cells and BEAS-2B cells. Data presented as mean ± SEM (n = 3); *p < 0.01 by one-way ANOVA.

(B) *SP* adhered to and invaded the PAFR-expressing cells (H226 and H1299). Bacteria were added to cells at a multiplicity of infection (MOI) of 10 for 1 h. The PspC-deficient mutant *SP* and heat-killed *SP* were defective for attachment and invasion compared to wild-type *SP* and the PspA-deficient mutant *SP*. *E. faecalis* did not attach to and invade lung cancer cells. Cells treated with PBS were used as negative controls. Data presented as mean ± SEM (n = 3); *p < 0.01 by one-way ANOVA.

(C) FISH analysis of *SP* using an Alexa Fluor 594-conjugated specific probe (Red) to *SP*. 4′,6-diamidino-2-phenylindole (DAPI) was used to visualize nuclear DNA of cells. Original magnification, X400. Three independent experiments were performed with consistent results. H460 and H1299 cells showed positive staining for *SP* (Red signals). Scale bar, 10 μm.

(D) The depletion of PAFR in H460 and H1299 cells by using siRNA reduced attachment and invasion of *SP*. Data presented as mean ± SEM (n = 3); *p < 0.01 by one-way ANOVA.

(E) The PAFR inhibitor, WEB2086, suppressed attachment and invasion of *SP* to H460 and H1299 cells in a dose-dependent manner (10, 30, and 60 μM and 1,000 μM WEB2086 were used). *p < 0.01.

(F) Enforced expression of PAFR in H226 cells increased attachment and invasion of wild-type *SP* and PspA-deficient mutant *SP*, but not PspC-deficient mutant *SP*. All the results are presented as the mean ± SD of three different experiments with triplicates. Data presented as mean ± SEM (n = 3); *p < 0.01 by one-way ANOVA.

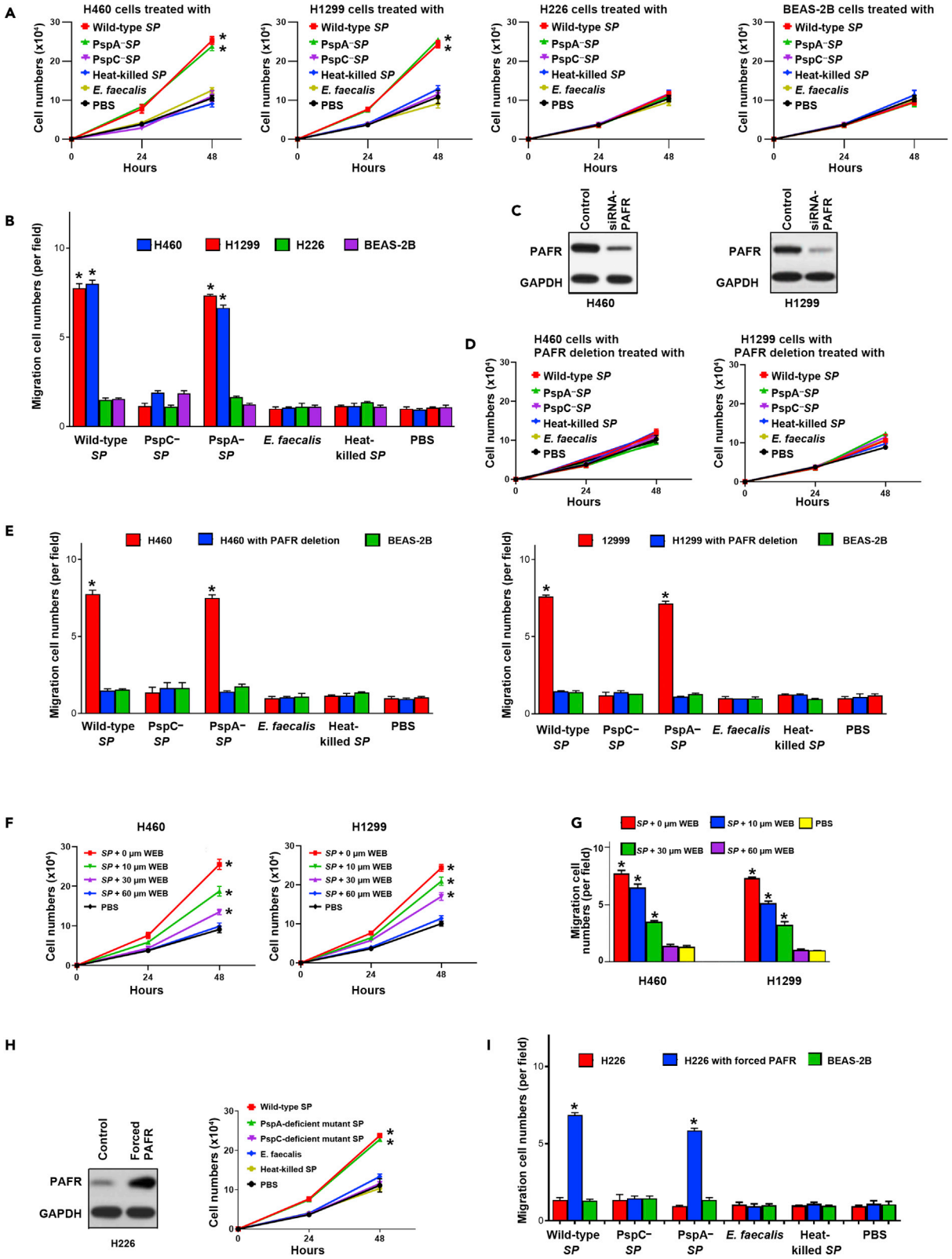
A
H460 cells treated with
H1299 cells treated with
H226 cells treated with
BEAS-2B cells treated with
Wild-type SP
PspA⁻SP
PspC⁻SP
Heat-killed SP
E. faecalis
PBS
Cell numbers (x10⁴)
Hours
B
H460
H1299
H226
BEAS-2B
Migration cell numbers (per field)
Wild-type SP
PspC⁻ SP
PspA⁻ SP
E. faecalis
Heat-killed SP
PBS
C
Control
siRNA-PAFR
PAFR
GAPDH
H460
H1299
D
H460 cells with PAFR deletion treated with
H1299 cells with PAFR deletion treated with
E
H460 with PAFR deletion
12999
H1299 with PAFR deletion
F
SP + 0 μm WEB
SP + 10 μm WEB
SP + 30 μm WEB
SP + 60 μm WEB
G
H
Forced PAFR
H226
Wild-type SP
PspA-deficient mutant SP
PspC-deficient mutant SP
E. faecalis
Heat-killed SP
I
H226
H226 with forced PAFR

Figure 2. *SP* promotes the tumorigenicity of lung cancer by integrating PspC and PAFR

(A) Wild-type and PspA-deficient mutant *SP*s stimulated proliferation of PAFR-expressing lung cancer cells (H460 and H1299) compared to untreated cells or those incubated with PspC-deficient mutant *SP*, heat-killed SP, and *E. faecalis*. Cells were incubated with bacteria at an MOI of 1000:1 for up to 48 h. Data presented as mean ± SEM (n = 3); *p < 0.01 by one-way ANOVA.

(B) Wild-type and PspA-deficient mutant *SP*s promoted migration of PAFR-expressing lung cancer cells, compared to untreated cells or those incubated with PspC-deficient mutant *SP*, heat-killed SP, and *E. faecalis* after 48-h treatment. Data presented as mean ± SEM (n = 3); *p < 0.01 by one-way ANOVA.

(C) siRNA was used to deplete PAFR in PAFR-expressing lung cancer cells, H460, and H1299 cells. Western blots showed that PAFR expression level was effectively reduced.

(D) *SP*-stimulated cell proliferation was inhibited by the depletion of PAFR in H460 and H1299 cells. Left panel showed the results of H460 cells with depletion of PAFR that were treated differently. Right panel displayed the results of H1299 cells with depletion of PAFR that were treated differently.

(E) *SP*-stimulated cell migration was suppressed by the depletion of PAFR in H460 and H1299. Data presented as mean ± SEM (n = 3); *p < 0.01 by one-way ANOVA. Red columns showed the results of H460 or H1299 cancer cells without depletion of PAFR. Blue columns indicated the results of H460 or H1299 cancer cells with depletion of PAFR. The depletion of PAFR in H460 and H1299 cancer cells decreased the effect of *SP* on cell migration.

(F) *SP*-stimulated cell proliferation of H460 and H1299 cells was inhibited by the PAFR inhibitor, WEB2086 (WEB), in a dose-dependent manner. Data presented as mean ± SEM (n = 3); *p < 0.01 by one-way ANOVA.

(G) *SP*-stimulated cell migration of H460 and H1299 was inhibited by WEB2086.

(H) H226 cells were forced to overexpress PAFR by using a PAFR-overexpressing plasmid. A vector expressing sequence lacking homology to the human genome databases was used as a control. *SP*-stimulated cell proliferation was elevated by enforced PAFR expression in the cells. Data presented as mean ± SEM (n = 3); *p < 0.01 by one-way ANOVA.

(I) *SP*-stimulated cell migration was elevated by enforced PAFR expression in H226 cells after 48 h treatment. Data presented as mean ± SEM (n = 3); *p < 0.01 by one-way ANOVA. The red column was wild-type H226 cancer cells that had a low expression level of PAFR. The blue column was H226 cancer cells with forced PAFR expression.

and NF-kB in H460 and H1299 cells (Figure 3A). However, the elimination of PAFR in H460 and H1299 cells decreased the *SP*-induced coactivation of PI3K, AKT, and NF-kB (Figure 3B). Furthermore, the deletion of PI3K, AKT, or NF-kB reduced the *SP*-stimulated cell proliferation in the cancer cells (Figure 3C). It is well established that NF-kB mediates induction of pro-inflammatory cytokines and plays tumor-promoting role of immune and inflammatory responses.[25–29] We further assessed pro-inflammatory cytokines in cancer cells infected with *SP*. *SP* significantly increased levels of eight cytokines (interleukin [IL]-1β, IL-4, IL-6, IL-8, IL-11, IL-12, tumor necrosis factor alpha [TNF-α], and monocyte chemoattractant protein-1 [MCP-1]) in H460 and H1299 cancer cells treated with *SP* compared with the controls (H460 and H1299 cancer cells treated with PBS) (Figure 3D). In contrast, the abolition of PAFR in H460 and H1299 cells decreased the *SP*-induced elevation of the cytokines (Figures S1A and S1B). Furthermore, H226 cells with forced expression of PAFR exhibited an increased level of PI3K, AKT, NF-kB, and the pro-inflammatory cytokines when treated with *SP* (Figures 3E and 3F). In addition, *SP* did not stimulate the pro-inflammatory cytokines in the H460 and H1299 cells with NF-kB depletion (Figures S2A and S2B). Altogether, *SP* infection could promote malignancy of lung cancer by activating PI3K/AKT and NF-kB oncogenic pathways and the activation-mediated inflammations.

SP promotes growth of lung tumor and induction of pro-inflammatory cytokines in xenograft animal models

We subcutaneously inoculated NSCLC cells (H460) with *SP* or PBS in BALB/C nude mice (five mice per group). Sixteen days postinjection, xenograft tumors were observed in all five mice injected with cancer cells treated with *SP* and in four of the five mice injected with cancer cells treated with PBS (Figure 4A). Furthermore, the tumors generated from cancer cells treated with *SP* were significantly larger compared to those created from cancer cells with PBS at the end of observation (days 28) (Figure 4B) (60.04 ± 14.11 mm^3 vs. 33.54 ± 9.02 mm^3, p = 0.0008). In addition, the tumors created from cancer cells treated with *SP* had higher levels of PAFR, PI3K, AKT, and NF-kB compared with the ones generated from cancer cells treated with PBS (Figure 4C). Moreover, the xenograft tumors created from the cancer cells treated with *SP* showed a higher level of pro-inflammatory cytokines (IL-4β, IL-6, IL-8, IL-11, IL-12, TNF-α, and transforming growth factor β [TGF-β]) compared with those generated from cancer cells treated with PBS (Figure 4D). The xenograft tumors generated from cancer cells infected with *SP* exhibited a higher level of proliferative marker (KI-67) compared to the controls (Figure 4C). The findings in ectopic xenograft mouse models are consistent with the above *in vitro* observations and further support the driving role of *SP* in lung tumorigenicity.

SP promotes the development of lung cancer and induces pro-inflammatory cytokines in a tobacco carcinogen-induced mouse lung cancer A/J model

Lung cancer is smoking-related disease.[1] Tobacco carcinogen could induce lung cancer in animal models.[31] To assess the role of *SP* infection in the development of NSCLC, A/J mice exposed to 4-(Methylnitrosamino)-1- (3-Pyridyl)-1-Butanone (NNK), a tobacco carcinogen, were treated with *SP* alone

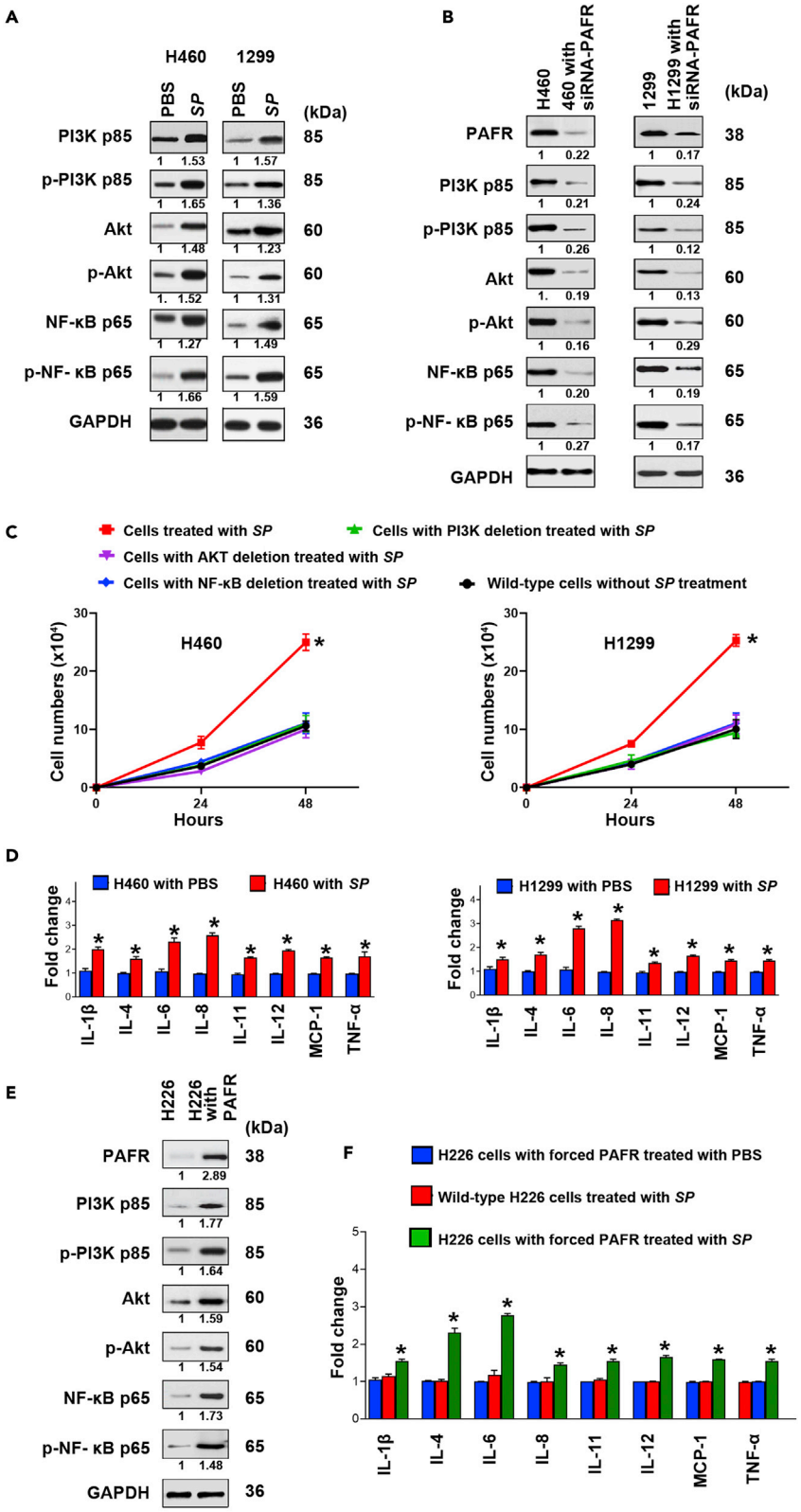
A
H460
1299
PBS
SP
PBS
SP
(kDa)
PI3K p85
p-PI3K p85
Akt
p-Akt
NF-κB p65
p-NF- κB p65
GAPDH
85
85
60
60
65
65
36
B
H460
460 with siRNA-PAFR
1299
H1299 with siRNA-PAFR
(kDa)
PAFR
PI3K p85
p-PI3K p85
Akt
p-Akt
NF-κB p65
p-NF- κB p65
GAPDH
38
85
85
60
60
65
65
36
C
Cells treated with SP
Cells with PI3K deletion treated with SP
Cells with AKT deletion treated with SP
Cells with NF-κB deletion treated with SP
Wild-type cells without SP treatment
H460
H1299
Cell numbers (x10⁴)
Hours
D
H460 with PBS
H460 with SP
H1299 with PBS
H1299 with SP
Fold change
IL-1β
IL-4
IL-6
IL-8
IL-11
IL-12
MCP-1
TNF-α
E
H226
H226 with PAFR
(kDa)
PAFR
PI3K p85
p-PI3K p85
Akt
p-Akt
NF-κB p65
p-NF- κB p65
GAPDH
38
85
85
60
60
65
65
36
F
H226 cells with forced PAFR treated with PBS
Wild-type H226 cells treated with SP
H226 cells with forced PAFR treated with SP
Fold change
IL-1β
IL-4
IL-6
IL-8
IL-11
IL-12
MCP-1
TNF-α

Figure 3. *SP* promotes lung tumorigenesis by stimulating PI3K/AKT and NF-kB signaling pathways

(A) PAFR-expressing H460 and H1299 cells treated with *SP* were analyzed by Western blot to determine expression of PI3K, AKT, and NF-kB. The cancer cells incubated with *SP* had higher expression levels of PI3K, AKT, and NF-kB compared with cells treated with PBS after 48 h treatment. Band intensity was determined by using ImageJ, and the ratio of each band was normalized to the corresponding GAPDH and shown below each band. *SP* activated PI3K, AKT, and NF-kB in H460 and H1299 cells.

(B) siRNA was used to deplete PAFR in H460 and H1299. The cells were treated with *SP*. SP-induced activations of PI3K, AKT, and NF-kB were inhibited by the depletion of PAFR in the cells. Data presented as mean ± SEM (n = 3); *p < 0.01 by one-way ANOVA.

(C) siRNA was used to deplete PI3K, AKT, and NF-kB in H460 and H1299, respectively. The deletion of PI3K, AKT, or NF-kB decreased the *SP*-stimulated cell proliferation in the cancer cells. Data presented as mean ± SEM (n = 3); *p < 0.01 by one-way ANOVA.

(D) PCR array was used to analyze the inflammatory cytokine gene expression. *SP* activated pro-inflammatory cytokines (IL-1β, IL-4, IL-6, IL-8, IL-11, IL-12, TNF-α, and MCP-1) (Red). Expression levels of the cytokines in the cells treated with PBS were designated as "1" (Blue). The results are presented as the mean ± SD of three different experiments with triplicates. Data presented as mean ± SEM (n = 3); *p < 0.01 by one-way ANOVA.

(E) Forced expression of PAFR in H226 cells was done by using PAFR-overexpressing plasmid. Enforced PAFR expression in the cancer cells increased SP-stimulated activations of PI3K, AKT, and NF-kB determined by Western Blots.

(F) Enforced PAFR expression in H226 cells activated cytokines in H226 cancer cells (Red). Expression levels of the cytokines in the H226 with forced PAFR expression treated with PBS (Blue) were designated as "1". Data presented as mean ± SEM (n = 3); *p < 0.01 by one-way ANOVA.

or *SP* and WEB2086. NNK-mice with *SP* administration had a significant increase in the number of lung tumors compared with NNK-mice without *SP* treatment or treated with *SP* and WEB2086 (Figures 5A–5E, and 5G) (3.00 ± 0.58 versus 1.10 ± 0.56 or 1.06 ± 0.73, All p < 0.05). The lung tumors created from mice treated with *SP* displayed histopathologic characteristics of lung adenocarcinomas (Figure 5F). To assess lung tumor burden, we euthanized 6 mice at week 24 with an overdose of CO2, harvested lungs, counted tumors, and measured the sizes. NNK-mice with *SP* administration had a significant increase in the number of lung tumors compared with mice without *SP* treatment or mice treated with *SP* and WEB2086 (All p < 0. 001) (5G). Furthermore, lung tumors in NNK-mice with *SP* administration were larger than those in mice without *SP* treatment or NNK-mice treated with *SP* and WEB2086 (41.82 ± 5.24 versus 10.34 ± 3.92 or 15.78 ± 6.06, All p < 0. 001) (5H). There was no statistical difference of tumor size in NNK-mice without *SP* treatment and NNK-mice treated with both SP and WEB2086 (10.34 ± 3.92 versus 15.78 ± 6.06, p = 0.166). In addition, droplet digital PCR (ddPCR) analysis showed that *SP* abundance in lung tumors of NNK-mice with *SP* treatment was significantly higher compared with that in NNK-mice without SP treatment (1.45 ± 0.306 versus 3.58 ± 0.623, p < 0.0001) (Figure S3). *SP* abundance in lung tumors of NNK-mice treated with both SP and WEB2086 was also significantly higher compared with that in NNK-mice without SP treatment (3.131 ± 0.676 versus 1.45 ± 0.306, p = 0.003). However, there was no statistical difference of *SP* abundance in lung tumors of NNK-mice treated with *SP* treatment alone and treated with both SP and WEB2086 (3.131 ± 0.676 versus 33.58 ± 0.623, p = 0.271). Moreover, mice treated with *SP* had a higher level of pro-inflammatory cytokines (IL-1β, IL-4, IL-6, IL-11, IL-12, 17A, interferon [IFN]-γ, and TGF-β) in their serum samples compared with mice without *SP* treatment or treated with both *SP* and WEB2086 (Figure 5I). Mice treated with *SP* had a shorter survival period compared to mice without *SP* treatment or mice treated with *SP* and WEB2086 (p < 0.05) (Figure 5J). The observations support that *SP* infection could initiate the development of lung tumors induced by the tobacco carcinogen and PAFR antagonist might prevent the tumor-promoting effects of *SP*.

Overabundance of SP correlates with high expression of PAFR in human NSCLC tissues and indicates poor clinical outcomes

To investigate clinical significance of *SP* infection, we determined DNA abundance of *SP* and RNA expression of PAFR by using ddPCR in 86 surgical NSCLC tissues and the paired normal lung tissues (Table 1). Both *Streptococcus* and PAFR displayed a higher level in lung tumor tissues compared with the corresponding noncancerous lung specimens (All p < 0.01) (Figures 6A and 6B). There was significant correlation between *SP* abundance and PAFR expression level in the lung tumor tissues (r = 0.758, p = 0.001) (Figure 6C). Furthermore, levels of *SP* in the tissue specimens were associated with advanced NSCLC stage (p = 0.026) but not with patient age, sex, or tumor histological type (all p > 0.05) (Table S1). In addition, univariate and multivariate analyses showed that abundance of *SP*, expression of PAFR, patient age, and tumor stage of NSCLC were significantly associated with disease-specific survival time of the patients (All p < 0.05) (Tables S2 and S3). Moreover, the patients with NSCLC were classified into two groups according

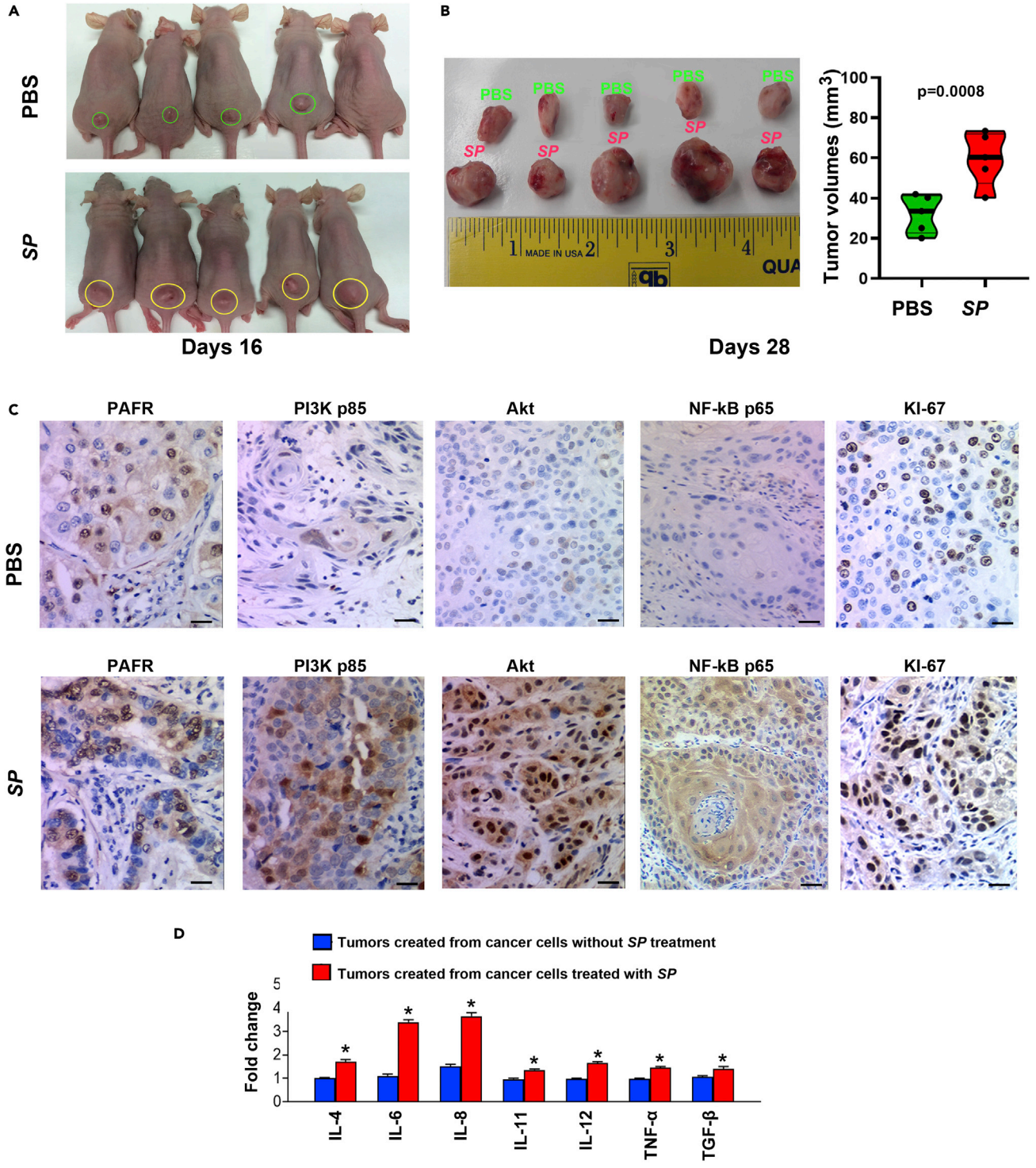

Figure 4. *SP* promotes tumorigenicity of NSCLC cells *in vivo*

(A) *SP*-treated H460 cells were subcutaneously injected into male BALB/C nude mice to generate xenograft animal model. On 16 days postinjection, tumors (yellow cycles) were founded in five mice injected with the cancer cells treated with *SP* and four (green cycles) of the five mice injected with the cancer cells treated with PBS.

(B) Xenograft tumors generated from mice inoculated with *SP*-treated H460 cells were considerably larger than those created from mice inoculated with PBS-treated H460 cells at the end of observation (days 28) Data presented as mean ± SEM (n = 4); *p = 0.0008 by one-way ANOVA. The tumor volumes of mice were measured using the formula v = (length [mm]) x (width [mm]) 2 × 0.52[64].

Figure 4. *Continued*

(C) Immunohistochemical staining patterns of PAFR, PI3K, AKT, NF-kB, and Ki-67 in the xenograft tumors generated from the cancer cells treated with PBS (top panel) and *SP* (bottom panel). Scale bar, 30 μm. Original magnification, X400.

(D) PCR array was used to analyze the inflammatory cytokine gene expression in tissue specimens. The xenograft tumors created from the cancer cells treated with *SP* showed a higher level of pro-inflammatory cytokines (IL-4β, IL-6, IL-8, IL-11, IL-12, TNF-α, and TGF-β) compared with those generated from cancer cells treated with PBS. Expression levels of the cytokines in the xenograft tumors created from the cancer cells treated without *SP* treatment were designated as "1". Data presented as mean ± SEM (n = 3); *$p < 0.01$ by one-way ANOVA.

to a median *SP* value (3.769) in lung tumor tissues. The Kaplan-Meier curve indicated that the lung cancer patients with higher abundance of *SP* (≥3.769) had poor disease-specific survival compared with those who had lower *SP* abundance (<3.769) ($p = 0.032$) (Figure 6D).

DISCUSSION

NSCLC is the leading cause of cancer-related deaths in men and women.[1] Although numerous bacterial aberrations are observed in lung tumors,[8–15,17] the causative role and molecular mechanism in promoting lung tumorigenesis remain unestablished. Here we find that *SP* infection could promote tumorigenicity of NSCLC by increasing the cell proliferation and migration. The tumor-promoting effect of *SP* is confirmed in ectopic xenograft mouse models. Furthermore, tobacco smoke carcinogen-treated A/J mice that are administrated with *SP* develop more lung tumors and have shorter survival times compared with mice treated with the carcinogen alone. In addition, *SP* is abundant in human lung tumor tissues in a manner of a stepwise increase from the early to advanced stages. Therefore, we report the evidence for oncogenic function of *SP* infection, instead of being simply a passenger, in the development and progression of NSCLC.

We investigate the underlying mechanism of *SP* infection in promoting carcinogenesis of NSCLC. *SP* selectively attaches to and invades PAFR-expressing lung cancer cells and further stimulates cell proliferation and migration in a PAFR-dependent manner. PAFR is associated with early malignant transformation and tumor metastasis of NSCLC.[32] PspA and PspC are two major pneumococcal surface proteins that play crucial roles in host cell attachment.[25] We find that PspC-deficient mutant *SP* loses the adhesion and invasion to PAFR-expressing lung cancer cells, suggesting that *SP* attachment and invasion to cancer cells require binding of PspC to PAFR. Furthermore, either PspC-deficient mutant *SP* or PAFR knockdown inhibits *SP* from binding and invading and hence abolishes the subsequent cell proliferation and migration. In addition, WEB2086, a PAFR antagonist, could inhibit *SP* from its binding and invading to cancer cells and obliterates the tumor-promoting effects. However, cancer cells infected with PspA-deficient mutant *SP* maintain the effects. Therefore, stimulating function of *SP* infection to promote lung tumorigenesis requires PsPC and PAFR and their interaction. *SP* might provide a preventive or therapeutic target for individuals at high risk to develop lung cancer or therapeutics of the disease.

PAFR directly regulates PI3K/AKT and NF-kB signaling pathways.[29,30] The PI3K/AKT pathway is one of the most frequently over-activated intracellular pathways by acting on downstream target proteins and contributes to the carcinogenesis, proliferation, invasion, and metastasis of tumor cells.[29] Furthermore, NF-kB plays an essential role in the cellular environment, immunity, inflammation, death, and cell proliferation.[30] Herein, we find that *SP* infection upregulates PI3K/AKT and NF-kB in PAFR-expressing lung cancer cells. Furthermore, reduced or forced expression of PAFR efficiently abolishes or increases the tumor-promoting function of *SP*, respectively. In addition, the deletion of PI3K, AKT, or NF-kB in cancer cells diminishes the effects of *SP* infection on the cell proliferation and migration. Consistently, *SP* infection promotes *in vivo* carcinogenicity of lung tumor xenografts that display high activations of PI3K/AKT and NF-kB oncogenic pathways. The mechanistic investigation is verified with tobacco smoke carcinogen-induced lung cancer animal models, whereby *SP* infection contributes to the development of lung cancer via the PI3K/AKT and NF-kB oncogenic pathways. Furthermore, PAFR antagonist could reduce *SP*-mediated PI3K/AKT, NF-kB, and cell proliferation in the lung cancer animal model, further supporting that the PspC and PAFR interaction is essential for the tumor-promoting effect of *SP*. Therefore, *SP* infection could play an oncogenic role in lung carcinogenesis by activating PI3K/AKT and NF-kB oncogenic pathways via binding PspC to PAFR.

Bacterial infection causes chronic inflammation, which leads to tumor development and progression.[14,16,27,29,30,33] Particularly, NF-kB activation plays tumor-promoting role of immune and inflammatory responses.[30] Our data show that pro-inflammatory cytokines are elevated in cancer cells infected with *SP*. Interestingly, the elimination of NF-kB significantly reduces pro-inflammatory cytokines in cancer

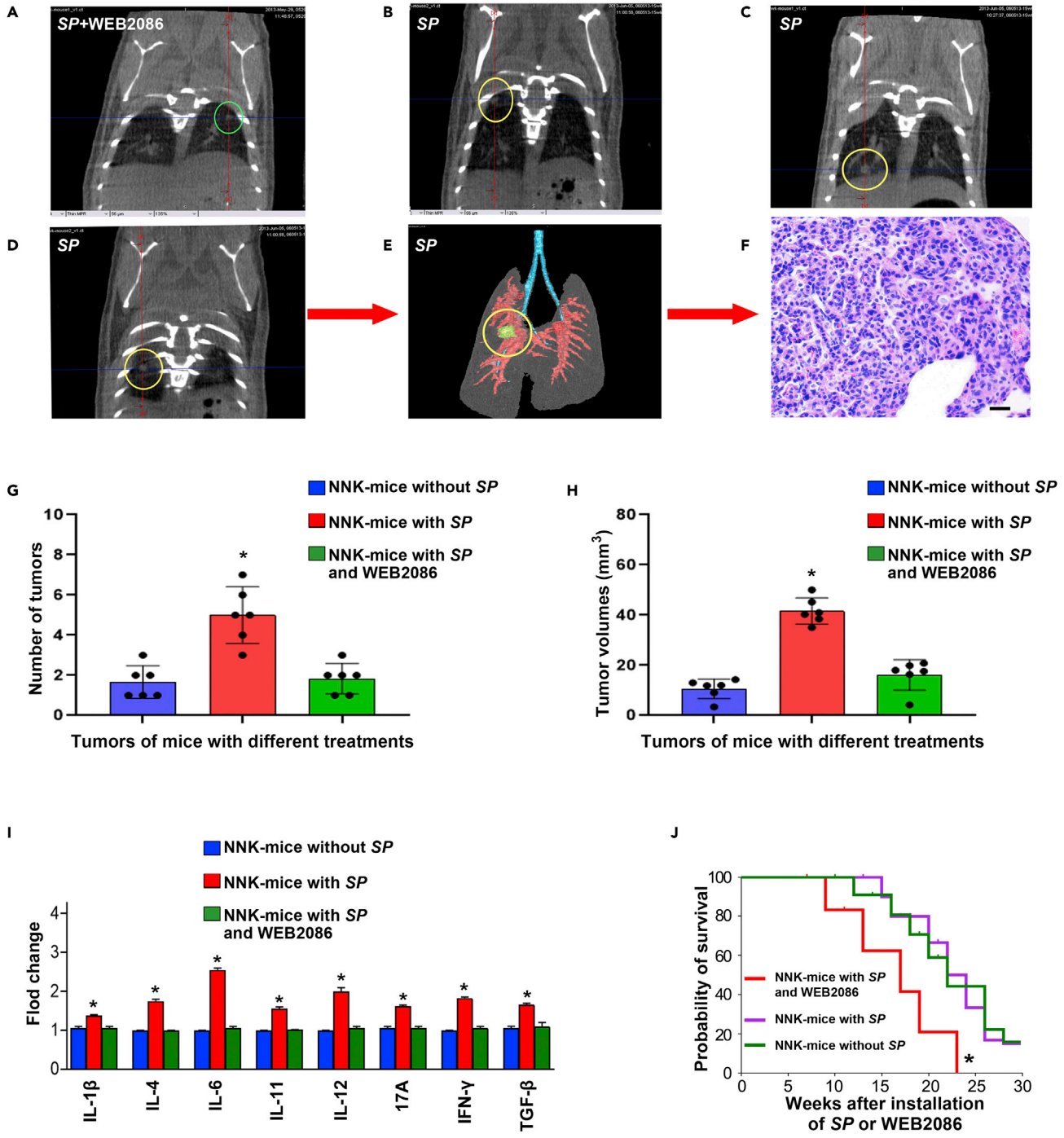

Figure 5. *SP* promotes the development of tobacco smoke-induced lung cancer in animals

(A) Representative micro-CT image of lungs of an NK-A/J mouse treated with *SP* and WEB2086 at week 14. A single lung tumor was identified (green circle).

(B–D) micro-CT scan slices highlighted multiple tumors (yellow circles) in a mouse treated with *SP* at week 14. (B–D) show of micro-CT images of lungs from the same mouse.

(E) 3D reconstruction of the lung tumor shown in (D).

(F) H & E-stained section from the mouse lungs shown in (E) displayed the histological characteristics of lung adenocarcinomas (magnification, ×200).Scale bar, 50 μm.

(G) NNK-mice with *SP* administration had a significant increase in the number of lung tumors compared with mice without *SP* treatment or mice treated with *SP* and WEB2086. Data presented as mean ± SEM (n = 3); *p < 0.01 by one-way ANOVA.

Figure 5. *Continued*

(H) Lung tumors of NNK-mice with *SP* administration were larger than those of NNK-mice without *SP* treatment or NNK-mice treated with *SP* and WEB2086. Data presented as mean ± SEM (n = 3); *p < 0.01 by one-way ANOVA.

(I) Mice treated with SP displayed a higher level of pro-inflammatory cytokines (IL-1β, IL-4, IL-6, IL-11, IL-12, 17A, IFN-γ, and TGF-β) in their serum compared with mice without SP treatment or treated with both SP and WEB2086. Expression levels of the cytokines in serum of the mice without *SP* treatment were designated as "1. FirePlex-96 Key Cytokines (Mouse) Immunoassay Panel was used to determine inflammatory cytokines in serum. The results are presented as the mean ± SD of three different experiments with triplicates. Data presented as mean ± SEM (n = 3); *p < 0.05 by one-way ANOVA.

(J) Kaplan-Meier survival curves of A/J mice with NNK-induced lung tumors treated with or without *SP* or SP and WEB2086, *p < 0.05, log rank (Mantel-Cox) test.

cells infected with *SP*. Furthermore, increased pro-inflammatory cytokines are also found in xenograft tumors created from cancer cells treated with *SP*. In addition, tobacco carcinogen-induced lung cancer mice treated with *SP* have higher levels of pro-inflammatory cytokines in serum compared with those treated with carcinogen alone. Of the increased pro-inflammatory cytokines, IL-6 and IL-8 level greatly elevated in cancer cell treated with *SP*, as compared with other cytokines. The results were confirmed in the xenograft tumors created from cancer cells treated with *SP*. The findings are consisted with previous discoveries that IL-6 and IL-8 might have important functions in promoting angiogenesis, tumor cell survival, chemoresistance, and migration.[34–37] Therefore, *SP* infection could activate NF-kB pathways and the induced inflammatory responses and hence plays an important role in the development and progression of lung cancer.

The high abundance of *SP* is frequently observed in 86 human lung tumor tissues, regardless of histological subtype. Furthermore, *SP* abundance is positively associated with levels of PAFR and stages of NSCLC and inversely correlated with disease-specific survival of the patients with lung cancer. The results obtained from the clinical specimens provide additional evidence to support that *SP* infection plays a crucial role in lung cancer development and progression. Although we cannot exclude that *SP* infection may directly contribute to the death of lung cancer patients, our finding is consistent with recent report that the microbes promote tumor progression and metastasis,[38] which is major cause for the death of lung cancer patients.

In sum, we identify *SP* as an oncogenic driver to promote the development and progression of lung cancer through interaction of its surface protein PspC with PAFR. The PspC-PAFR interaction initiates *SP* adhesion and activates PI3K/AKT and NF-kB signaling pathways and the activation-mediated inflammatory responses and hence contributes to lung tumorigenicity. The discoveries would open new horizons to target

Table 1. Demographic and clinical characteristics of 86 NSCLC patients

Characteristics	No. of patients
Age at diagnosis	67.5 ± 8.7
Sex	
Male	56
Female	30
Race	
White	60
Black	26
Smoker	
Yes	77
No	9
Tumor histology	
Adenocarcinoma	46
Squamous cell carcinoma	40
T stage	
I	20
II	37
III-IV	29

NSCLC, non-small cell lung cancer.

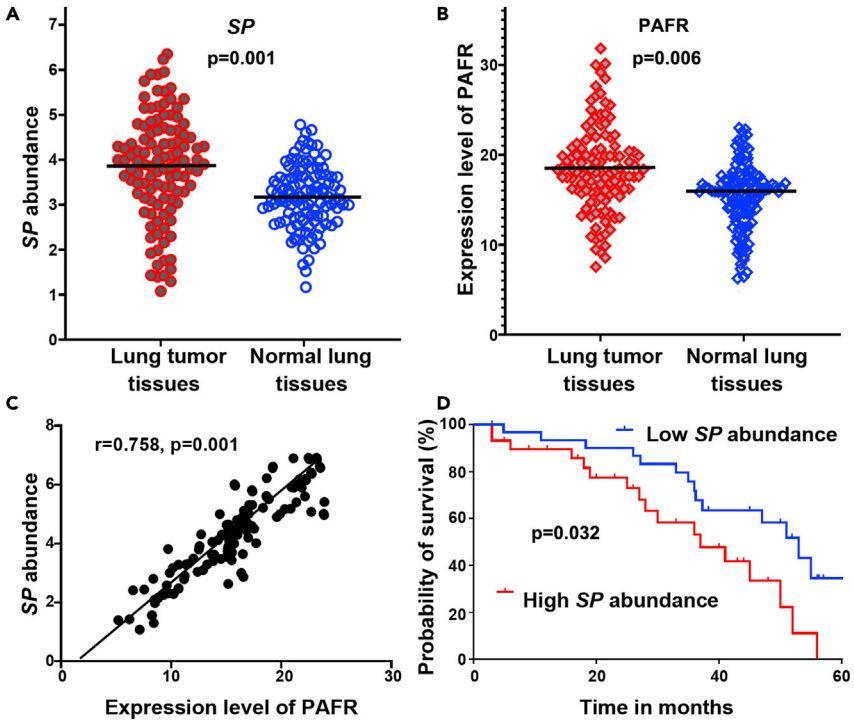

Figure 6. *SP* is overrepresented in lung tumor tissues, associated with PAFR expression, and inversely correlated with disease-specific survival of the patients with NSCLC

(A) *SP* was overabundant in lung tumor tissues compared with the corresponding noncancerous lung specimens Data presented as mean ± SEM; *p = 0.001 by one-way ANOVA. Amount of *SP* was determined by ddPCR and represented by copies of DNA/μL PCR reaction per sample.

(B) A higher expression level of PAFR was found in lung tumor tissues compared with the corresponding noncancerous lung specimens. Data presented as mean ± SEM; *p = 0.006 by one-way ANOVA. Expression level of PAFR was determined by ddPCR and represented by copies of RNA/μL PCR reaction per sample.

(C) The amount of *SP* was positively associated with PAFR expression in cancer tissues (n = 138, p = 0.001 by 2-tailed nonparametric Spearman correlation).

(D) Kaplan-Meier survival curve for 86 clinical specimens showed overabundance of *SP* was associated with poor disease-specific survival in lung cancer patients (log rank (Mantel-Cox) test). p = 0.032.

microbiota for the prevention, diagnosis, and treatment of lung cancer and thus have important clinical implications.

Limitations of the study

First, it is well known that actionable mutations, such as epidermal growth factor receptor (EGFR) and anaplastic lymphoma kinase (ALK), lead to unregulated proliferation and survival of tumor cells and associated with advanced NSCLC stages. It might be interesting to evaluate the collection between status of the actionable mutations and bacterial abundances in lung cancer. Because most of the actionable mutation statuses are not available from the patients, in this present study, we are not able to perform this analysis. However, we are not collecting new lung tumor specimens with the associated actionable mutations to investigate the correlation between *SP* abundance and actionable mutations and patients' responses to treatments. Second, clinically, the most common immediate cause of death of lung cancer patients is the extensive widespread metastases. The microbes can travel through the circulatory system with the cancer cells and play critical roles in tumor metastasis.[38] Therefore, *SP* could modulate and promote cancer cell survival, interact with the immune system, and contribute to tumor metastasis, ultimately causing the death of lung cancer patients. Other causes for the death of lung cancer patients include infection. Therefore, we cannot exclude that *SP* infection may directly contribute to the death of lung cancer patients. However, how many of lung cancer patients died directly from bacterial infection are not available in this current study. We will perform a different study to investigate if *SP* infection directly causes the death of lung cancer patients by recruiting new lung cancer cases and following their outcomes.

STAR★METHODS

Detailed methods are provided in the online version of this paper and include the following:

- KEY RESOURCES TABLE
- RESOURCE AVAILABILITY
  - Lead contact
  - Materials availability
  - Data and code availability
- EXPERIMENTAL MODEL AND SUBJECT DETAILS
  - Bacterial strain and culture conditions
  - Cell culture
  - Clinical specimens
- METHOD DETAILS
  - Cell adhesion and invasion assays
  - RNAi
  - Construction of mutants
  - Ectopic PAFR expression
  - Cell proliferation and migration assays
  - Immunohistochemistry and Western blotting
  - PCR array analysis of pro-inflammatory cytokine gene expression
  - Pro-inflammatory cytokines analysis
  - FISH
  - Droplet digital PCR (ddPCR) analysis of DNA abundance of SP and mRNA expression of PAFR
  - Tumorigenicity sssay in nude mice
  - A tobacco carcinogen–induced mouse lung cancer model
  - Micro-CT images of the tobacco carcinogen–induced mouse lung cancer A/J model
- QUANTIFICATION AND STATISTICAL ANALYSIS

SUPPLEMENTAL INFORMATION

Supplemental information can be found online at https://doi.org/10.1016/j.isci.2022.105923.

ACKNOWLEDGMENTS

We thank the University of Maryland Marlene and Stewart Greenebaum Comprehensive Cancer Center Biostatistics Shared Service for providing statistical analysis services. This work was supported in part by National Cancer Institute grant CA-UH2-229132 and U.S. Food and Drug Administration grant-U01FD005946 (FJ).

AUTHOR CONTRIBUTIONS

N.L., H.Z., and P.D. conducted experiments and participated in data interpretation. V.H., P.D., J.D., and N.W.T. collected samples. F.J. designed research approaches and participated in data interpretation. V.H. and F.J. prepared the manuscript. All authors read and approved the final manuscript.

DECLARATION OF INTERESTS

The authors declare no competing interests.

ETHICAL APPROVAL AND CONSENT TO PARTICIPATE

All work was approved by the Ethics Committee of University of Maryland Baltimore Consent for publication.

Received: April 18, 2022
Revised: November 12, 2022
Accepted: December 30, 2022
Published: February 17, 2023

REFERENCES

1. National Lung Screening Trial Research Team, Aberle, D.R., Adams, A.M., Berg, C.D., Black, W.C., Clapp, J.D., Fagerstrom, R.M., Gareen, I.F., Gatsonis, C., Marcus, P.M., and Sicks, J.D. (2011). Reduced lung-cancer mortality with low-dose computed tomographic screening. N. Engl. J. Med. *365*, 395–409.

2. Garrett, W.S. (2015). Cancer and the microbiota. Science *348*, 80–86.

3. Mao, Q., Jiang, F., Yin, R., Wang, J., Xia, W., Dong, G., Ma, W., Yang, Y., Xu, L., and Hu, J. (2018). Interplay between the lung microbiome and lung cancer. Cancer Lett. *415*, 40–48.

4. Wang, K., Huang, Y., Zhang, Z., Liao, J., Ding, Y., Fang, X., Liu, L., Luo, J., and Kong, J. (2019). A preliminary study of microbiota diversity in saliva and bronchoalveolar lavage fluid from patients with primary bronchogenic carcinoma. Med. Sci. Monit. *25*, 2819–2834.

5. Hogan, D.A., Willger, S.D., Dolben, E.L., Hampton, T.H., Stanton, B.A., Morrison, H.G., Sogin, M.L., Czum, J., and Ashare, A. (2016). Analysis of lung microbiota in bronchoalveolar lavage, protected brush and sputum samples from subjects with mild-to-moderate cystic fibrosis lung disease. PLoS One *11*, e0149998.

6. Novick, S., Shagan, M., Blau, K., Lifshitz, S., Givon-Lavi, N., Grossman, N., Bodner, L., Dagan, R., and Mizrachi Nebenzahl, Y. (2017). Adhesion and invasion of Streptococcus pneumoniae to primary and secondary respiratory epithelial cells. Mol. Med. Rep. *15*, 65–74.

7. Kovaleva, O.V., Romashin, D., Zborovskaya, I.B., Davydov, M.M., Shogenov, M.S., and Gratchev, A. (2019). Human lung microbiome on the way to cancer. J. Immunol. Res. *2019*, 1394191.

8. Peters, B.A., Hayes, R.B., Goparaju, C., Reid, C., Pass, H.I., and Ahn, J. (2019). The microbiome in lung cancer tissue and recurrence-free survival. Cancer Epidemiol. Biomarkers Prev. *28*, 731–740.

9. Yu, G., Gail, M.H., Consonni, D., Carugno, M., Humphrys, M., Pesatori, A.C., Caporaso, N.E., Goedert, J.J., Ravel, J., and Landi, M.T. (2016). Characterizing human lung tissue microbiota and its relationship to epidemiological and clinical features. Genome Biol. *17*, 163.

10. Liu, H.X., Tao, L.L., Zhang, J., Zhu, Y.G., Zheng, Y., Liu, D., Zhou, M., Ke, H., Shi, M.M., and Qu, J.M. (2018a). Difference of lower airway microbiome in bilateral protected specimen brush between lung cancer patients with unilateral lobar masses and control subjects. Int. J. Cancer *142*, 769–778.

11. Apopa, P.L., Alley, L., Penney, R.B., Arnaoutakis, K., Steliga, M.A., Jeffus, S., Bircan, E., Gopalan, B., Jin, J., Patumcharoenpol, P., et al. (2018). PARP1 is up-regulated in non-small cell lung cancer tissues in the presence of the cyanobacterial toxin microcystin. Front. Microbiol. *9*, 1757.

12. Liu, Y., O'Brien, J.L., Ajami, N.J., Scheurer, M.E., Amirian, E.S., Armstrong, G., Tsavachidis, S., Thrift, A.P., Jiao, L., Wong, M.C., et al. (2018b). Lung tissue microbial profile in lung cancer is distinct from emphysema. Am. J. Cancer Res. *8*, 1775–1787.

13. Lee, S.H., Sung, J.Y., Yong, D., Chun, J., Kim, S.Y., Song, J.H., Chung, K.S., Kim, E.Y., Jung, J.Y., Kang, Y.A., et al. (2016). Characterization of microbiome in bronchoalveolar lavage fluid of patients with lung cancer comparing with benign mass like lesions. Lung Cancer *102*, 89–95.

14. Tsay, J.C.J., Wu, B.G., Badri, M.H., Clemente, J.C., Shen, N., Meyn, P., Li, Y., Yie, T.A., Lhakhang, T., Olsen, E., et al. (2018). Airway microbiota is associated with upregulation of the PI3K pathway in lung cancer. Am. J. Respir. Crit. Care Med. *198*, 1188–1198.

15. Jin, J., Gan, Y., Liu, H., Wang, Z., Yuan, J., Deng, T., Zhou, Y., Zhu, Y., Zhu, H., Yang, S., et al. (2019). Diminishing microbiome richness and distinction in the lower respiratory tract of lung cancer patients: a multiple comparative study design with independent validation. Lung Cancer *136*, 129–135.

16. Tsay, J.C.J., Wu, B.G., Sulaiman, I., Gershner, K., Schluger, R., Li, Y., Yie, T.A., Meyn, P., Olsen, E., Perez, L., et al. (2021). Lower airway dysbiosis affects lung cancer progression. Cancer Discov. *11*, 293–307.

17. Greathouse, K.L., White, J.R., Vargas, A.J., Bliskovsky, V.V., Beck, J.A., von Muhlinen, N., Polley, E.C., Bowman, E.D., Khan, M.A., Robles, A.I., et al. (2020). Interaction between the microbiome and TP53 in human lung cancer. Genome Biol. *21*, 41.

18. Sepich-Poore, G.D., Zitvogel, L., Straussman, R., Hasty, J., Wargo, J.A., and Knight, R. (2021). The microbiome and human cancer. Science *371*, eabc4552.

19. Pasquereau-Kotula, E., Martins, M., Aymeric, L., and Dramsi, S. (2018). Significance of Streptococcus gallolyticus subsp. gallolyticus association with colorectal cancer. Front. Microbiol. *9*, 614.

20. Bello, S., Vengoechea, J.J., Ponce-Alonso, M., Figueredo, A.L., Mincholé, E., Rezusta, A., et al. (2020). Core microbiota in central lung cancer with streptococcal enrichment as a possible diagnostic marker. Arch. Bronconeumol. *57*, 681–689.

21. Cundell, D.R., Gerard, N.P., Gerard, C., Idanpaan-Heikkila, I., and Tuomanen, E.I. (1995). Streptococcus pneumoniae anchor to activated human cells by the receptor for platelet-activating factor. Nature *377*, 435–438.

22. Mushtaq, N., Ezzati, M., Hall, L., Dickson, I., Kirwan, M., Png, K.M.Y., Mudway, I.S., and Grigg, J. (2011). Adhesion of Streptococcus pneumoniae to human airway epithelial cells exposed to urban particulate matter. J. Allergy Clin. Immunol. *127*, 1236–1242.e2.

23. Grigg, J., Walters, H., Sohal, S.S., Wood-Baker, R., Reid, D.W., Xu, C.B., Edvinsson, L., Morissette, M.C., Stämpfli, M.R., Kirwan, M., et al. (2012). Cigarette smoke and platelet-activating factor receptor dependent adhesion of Streptococcus pneumoniae to lower airway cells. Thorax *67*, 908–913.

24. Chen, J., Lan, T., Zhang, W., Dong, L., Kang, N., Zhang, S., Fu, M., Liu, B., Liu, K., and Zhan, Q. (2015a). Feed-forward reciprocal activation of PAFR and STAT3 regulates epithelial-mesenchymal transition in non-small cell lung cancer. Cancer Res. *75*, 4198–4210.

25. Marquart, M.E. (2021). Pathogenicity and virulence of Streptococcus pneumoniae: cutting to the chase on proteases. Virulence *12*, 766–787.

26. Chen, J., Lan, T., Zhang, W., Dong, L., Kang, N., Zhang, S., Fu, M., Liu, B., Liu, K., Zhang, C., et al. (2015b). Platelet-activating factor receptor-mediated PI3K/AKT activation contributes to the malignant development of esophageal squamous cell carcinoma. Oncogene *34*, 5114–5127.

27. Sanchez, A., and Villanueva, J. (2010). PI3K-based molecular signatures link high PI3K pathway activity with low ER levels in ER+ breast cancer. Expert Rev. Proteomics *7*, 819–821.

28. Creighton, C.J., Fu, X., Hennessy, B.T., Casa, A.J., Zhang, Y., Gonzalez-Angulo, A.M., Lluch, A., Gray, J.W., Brown, P.H., Hilsenbeck, S.G., et al. (2010). Proteomic and transcriptomic profiling reveals a link between the PI3K pathway and lower estrogen-receptor (ER) levels and activity in ER+ breast cancer. Breast Cancer Res. *12*, R40.

29. Fruman, D.A., Chiu, H., Hopkins, B.D., Bagrodia, S., Cantley, L.C., and Abraham, R.T. (2017). The PI3K pathway in human disease. Cell *170*, 605–635.

30. Karin, M. (2009). NF-kappaB as a critical link between inflammation and cancer. Cold Spring Harb. Perspect. Biol. *1*, a000141.

31. Ge, G.Z., Xu, T.R., and Chen, C. (2015). Tobacco carcinogen NNK-induced lung cancer animal models and associated carcinogenic mechanisms. Acta Biochim. Biophys. Sin. *47*, 477–487.

32. de Oliveira, S.I., Andrade, L.N.S., Onuchic, A.C., Nonogaki, S., Fernandes, P.D., Pinheiro, M.C., Rohde, C.B.S., Chammas, R., and Jancar, S. (2010). Platelet-activating factor receptor (PAF-R)-dependent pathways control tumour growth and tumour response to chemotherapy. BMC Cancer *10*, 200.

33. Kumar, R., Herold, J.L., Schady, D., Davis, J., Kopetz, S., Martinez-Moczygemba, M., Murray, B.E., Han, F., Li, Y., Callaway, E., et al. (2017). Streptococcus gallolyticus subsp. gallolyticus promotes colorectal tumor development. PLoS Pathog. *13*, e1006440.

34. Ryan, B.M., Pine, S.R., Chaturvedi, A.K., Caporaso, N., and Harris, C.C. (2014). A combined prognostic serum interleukin-8 and interleukin-6 classifier for stage 1 lung

cancer in the prostate, lung, colorectal, and ovarian cancer screening trial. J. Thorac. Oncol. *9*, 1494–1503.

35. Chang, C.H., Hsiao, C.F., Yeh, Y.M., Chang, G.C., Tsai, Y.H., Chen, Y.M., Huang, M.S., Chen, H.L., Li, Y.J., Yang, P.C., et al. (2013). Circulating interleukin-6 level is a prognostic marker for survival in advanced nonsmall cell lung cancer patients treated with chemotherapy. Int. J. Cancer *132*, 1977–1985.

36. Guo, Y., Xu, F., Lu, T., Duan, Z., and Zhang, Z. (2012). Interleukin-6 signaling pathway in targeted therapy for cancer. Cancer Treat Rev. *38*, 904–910.

37. Waugh, D.J.J., and Wilson, C. (2008). The interleukin-8 pathway in cancer. Clin. Cancer Res. *14*, 6735–6741.

38. Fu, A., Yao, B., Dong, T., Chen, Y., Yao, J., Liu, Y., Li, H., Bai, H., Liu, X., Zhang, Y., et al. (2022). Tumor-resident intracellular microbiota promotes metastatic colonization in breast cancer. Cell *185*, 1356–1372.e26.

39. Gou, X., Zhang, Q., More, S., Bamunuarachchi, G., Liang, Y., Haider Khan, F., Maranville, R., Zuniga, E., Wang, C., and Liu, L. (2019). Repeated exposure to streptococcus pneumoniae exacerbates chronic obstructive pulmonary disease. Am. J. Pathol. *189*, 1711–1720.

40. Rabiei, P., Mohabatkar, H., and Behbahani, M. (2019). Studying the effects of several heat-inactivated bacteria on colon and breast cancer cells. Mol. Biol. Res. Commun. *8*, 91–98.

41. Fan, T., Li, R., Todd, N.W., Qiu, Q., Fang, H.B., Wang, H., Shen, J., Zhao, R.Y., Caraway, N.P., Katz, R.L., et al. (2007). Up-regulation of 14-3-3zeta in lung cancer and its implication as prognostic and therapeutic target. Cancer Res. *67*, 7901–7906.

42. Jiang, F., Qiu, Q., Khanna, A., Todd, N.W., Deepak, J., Xing, L., Wang, H., Liu, Z., Su, Y., Stass, S.A., and Katz, R.L. (2009). Aldehyde dehydrogenase 1 is a tumor stem cell-associated marker in lung cancer. Mol. Cancer Res. *7*, 330–338.

43. Mei, Y.P., Liao, J.P., Shen, J., Yu, L., Liu, B.L., Liu, L., Li, R.Y., Ji, L., Dorsey, S.G., Jiang, Z.R., et al. (2012). Small nucleolar RNA 42 acts as an oncogene in lung tumorigenesis. Oncogene *31*, 2794–2804.

44. Mannoor, K., Shen, J., Liao, J., Liu, Z., and Jiang, F. (2014). Small nucleolar RNA signatures of lung tumor-initiating cells. Mol. Cancer *13*, 104.

45. Hammerschmidt, S., Agarwal, V., Kunert, A., Haelbich, S., Skerka, C., and Zipfel, P.F. (2007). The host immune regulator factor H interacts via two contact sites with the PspC protein of Streptococcus pneumoniae and mediates adhesion to host epithelial cells. J. Immunol. *178*, 5848–5858.

46. Iannelli, F., Chiavolini, D., Ricci, S., Oggioni, M.R., and Pozzi, G. (2004). Pneumococcal surface protein C contributes to sepsis caused by Streptococcus pneumoniae in mice. Infect. Immun. *72*, 3077–3080.

47. Janulczyk, R., Iannelli, F., Sjoholm, A.G., Pozzi, G., and Bjorck, L. (2000). Hic, a novel surface protein of Streptococcus pneumoniae that interferes with complement function. J. Biol. Chem. *275*, 37257–37263.

48. Hermans, P.W.M., Adrian, P.V., Albert, C., Estevão, S., Hoogenboezem, T., Luijendijk, I.H.T., Kamphausen, T., and Hammerschmidt, S. (2006). The streptococcal lipoprotein rotamase A (SlrA) is a functional peptidyl-prolyl isomerase involved in pneumococcal colonization. J. Biol. Chem. *281*, 968–976.

49. Wang, J., Tian, X., Han, R., Zhang, X., Wang, X., Shen, H., Xue, L., Liu, Y., Yan, X., Shen, J., et al. (2014). Downregulation of miR-486-5p contributes to tumor progression and metastasis by targeting protumorigenic ARHGAP5 in lung cancer. Oncogene *33*, 1181–1189.

50. Long, X., Wong, C.C., Tong, L., Chu, E.S.H., Ho Szeto, C., Go, M.Y.Y., Coker, O.O., Chan, A.W.H., Chan, F.K.L., Sung, J.J.Y., and Yu, J. (2019). Peptostreptococcus anaerobius promotes colorectal carcinogenesis and modulates tumour immunity. Nat. Microbiol. *4*, 2319–2330.

51. Kostic, A.D., Gevers, D., Pedamallu, C.S., Michaud, M., Duke, F., Earl, A.M., Ojesina, A.I., Jung, J., Bass, A.J., Tabernero, J., et al. (2012). Genomic analysis identifies association of Fusobacterium with colorectal carcinoma. Genome Res. *22*, 292–298.

52. Gescher, D.M., Kovacevic, D., Schmiedel, D., Siemoneit, S., Mallmann, C., Halle, E., Göbel, U.B., and Moter, A. (2008). Fluorescence in situ hybridisation (FISH) accelerates identification of Gram-positive cocci in positive blood cultures. Int. J. Antimicrob. Agents *32*, S51–S59.

53. Li, N., Ma, J., Guarnera, M.A., Fang, H., Cai, L., and Jiang, F. (2014). Digital PCR quantification of miRNAs in sputum for diagnosis of lung cancer. J. Cancer Res. Clin. Oncol. *140*, 145–150.

54. Ma, J., Li, N., Guarnera, M., and Jiang, F. (2013). Quantification of plasma miRNAs by digital PCR for cancer diagnosis. Biomark. Insights *8*, 127–136.

55. Su, Y., Fang, H., and Jiang, F. (2016). Integrating DNA methylation and microRNA biomarkers in sputum for lung cancer detection. Clin. Epigenetics *8*, 109.

56. Su, Y., Fang, H.B., and Jiang, F. (2018). An epigenetic classifier for early stage lung cancer. Clin. Epigenetics *10*, 68.

57. Li, H., Jiang, Z., Leng, Q., Bai, F., Wang, J., Ding, X., Li, Y., Zhang, X., Fang, H., Yfantis, H.G., et al. (2017). A prediction model for distinguishing lung squamous cell carcinoma from adenocarcinoma. Oncotarget *8*, 50704–50714.

58. Ma, J., Mannoor, K., Gao, L., Tan, A., Guarnera, M.A., Zhan, M., Shetty, A., Stass, S.A., Xing, L., and Jiang, F. (2014). Characterization of microRNA transcriptome in lung cancer by next-generation deep sequencing. Mol. Oncol. *8*, 1208–1219.

59. Lin, Y., Holden, V., Dhilipkannah, P., Deepak, J., Todd, N.W., and Jiang, F. (2020). A non-coding RNA landscape of bronchial epitheliums of lung cancer patients. Biomedicines *8*, 88.

60. Lin, Y., Leng, Q., Zhan, M., and Jiang, F. (2018). A plasma long noncoding RNA signature for early detection of lung cancer. Transl. Oncol. *11*, 1225–1231.

61. Leng, Q., Tsou, J.H., Zhan, M., and Jiang, F. (2018). Fucosylation genes as circulating biomarkers for lung cancer. J. Cancer Res. Clin. Oncol. *144*, 2109–2115.

62. Coskun-Ari, F.F., Guldemir, D., and Durmaz, R. (2012). One-step multiplex PCR assay for detecting Streptococcus pneumoniae serogroups/types covered by 13-valent pneumococcal conjugate vaccine (PCV13). PLoS One *7*, e50406.

63. Li, N., Dhilipkannah, P., and Jiang, F. (2021). High-throughput detection of multiple miRNAs and methylated DNA by droplet digital PCR. J. Pers. Med. *11*, 359.

64. Li, M., Zhang, Y., Liu, Z., Bharadwaj, U., Wang, H., Wang, X., Zhang, S., Liuzzi, J.P., Chang, S.M., Cousins, R.J., et al. (2007). Aberrant expression of zinc transporter ZIP4 (SLC39A4) significantly contributes to human pancreatic cancer pathogenesis and progression. Proc. Natl. Acad. Sci. USA *104*, 18636–18641.

65. Yu, Y., Zhang, M., Zhang, X., Cai, Q., Hong, S., Jiang, W., and Xu, C. (2014). Synergistic effects of combined platelet-activating factor receptor and epidermal growth factor receptor targeting in ovarian cancer cells. J. Hematol. Oncol. *7*, 39.

66. Rudyanto, R.D., Bastarrika, G., de Biurrun, G., Agorreta, J., Montuenga, L.M., Ortiz-de-Solorzano, C., and Muñoz-Barrutia, A. (2013). Individual nodule tracking in micro-CT images of a longitudinal lung cancer mouse model. Med. Image Anal. *17*, 1095–1105.

67. Foster, W.K., and Ford, N.L. (2011). Investigating the effect of longitudinal micro-CT imaging on tumour growth in mice. Phys. Med. Biol. *56*, 315–326.

68. Haines, B.B., Bettano, K.A., Chenard, M., Sevilla, R.S., Ware, C., Angagaw, M.H., Winkelmann, C.T., Tong, C., Reilly, J.F., Sur, C., and Zhang, W. (2009). A quantitative volumetric micro-computed tomography method to analyze lung tumors in genetically engineered mouse models. Neoplasia *11*, 39–47.

STAR★METHODS

KEY RESOURCES TABLE

REAGENT or RESOURCE	SOURCE	IDENTIFIER
Antibodies		
Rabbit polyclonal to PAF-R	Abcam	ab104162
Anti-PI 3 Kinase p85 alpha antibody	Abcam	ab191606
Anti-PI 3 Kinase p85 alpha [EP380Y]	Abcam	ab40755
Anti-AKT antibody	Abcam	ab8805
Anti-AKT1 (phospho S473) antibody [EP2109Y]	Abcam	ab81283
Anti-NF-kB p65 antibody	Abcam	ab16502
Anti-AKT1 (phospho S473) antibody [EP2109Y]	Abcam	ab81283
Anti-GAPDH antibody	Abcam	ab9485
Bacterial and virus strains		
S pneumoniae	NCTC	NCTC10319
E. faecalis	ATCC	BAA-2128
Biological samples		
Human lung tumor and normal lung tissues	University of Maryland Medical Center	N/A
Chemicals, peptides, and recombinant proteins		
PBS (PBS)	Sigma-Aldrich	P5493
Dulbecco's Modified Eagle Medium (DMEM)	Sigma-Aldrich	SLM-241
Triton X-100	Sigma-Aldrich	8482
Penicillin	Sigma-Aldrich	113-98-4
Gentamicin	Sigma-Aldrich	1405-41-0
Trypsin	Sigma-Aldrich	T4549
EDTA	Sigma-Aldrich	200-449-4
Saponin	Sigma-Aldrich	8047-15-2
WEB2086 (Apafant)	Sigma-Aldrich	105219-56-5
Opti-MEM medium	Thermo Fisher	31985088
LipofectamineTM RNAiMAX	Thermo Fisher	13778150
Erythromycin	Sigma-Aldrich	114-07-8
Lipofectamine 2000	Sigma-Aldrich	F0895
Crystal violet	Sigma-Aldrich	548-62-9
Lysozyme	Sigma-Aldrich	235-747-3
Lysostaphin	Sigma-Aldrich	9011-93-2
2-(4-Amidinophenyl)-6-indolecarbamidine (DAPI)	Sigma-Aldrich	28718-90-3
ddPCR Supermix	Bio-Rad	1863024
Piperacillin	Sigma-Aldrich	66258-76-2
Pentobarbital	Sigma-Aldrich	200-323-9
4-(Methylnitrosamino)-1- (3-Pyridyl)-1-Butanone (NNK)	Sigma-Aldrich	64091-91-4
Critical commercial assays		
Dako envision dual link system-HRP (DAB+)	Dako	K4065
RT2 Profiler PCR Array for inflammatory cytokines	QIAGEN	330231

(*Continued on next page*)

Continued

REAGENT or RESOURCE	SOURCE	IDENTIFIER
FirePlex®-96 Key Cytokines Immunoassay Panel	Abcam	ab235656
QIAGEN RNA preparation kit	QIAGEN	80284
Experimental models: Cell lines		
NCI-H226	ATCC	CRL-5826
NCI-H460	ATCC	HTB-177
NCI-H1299	ATCC	CRL-5803
BEAS-2B	ATCC	CRL-9609
Experimental models: Organisms/strains		
Male nude mice (BALB/C)	Charles River Laboratories	CAnN.Cg-Foxn1nu/Crl
Female A/J mice	The Jackson Laboratory	000646
Oligonucleotides		
siRNAs targeting PARF, PI3K, AKT, and NF-kB	This paper	N/A
PCR primers for PspC or PsaA	This paper	N/A
Alexa Fluor 594-conjugated specific probe for *S pneumoniae*	This paper	N/A
PCR primers for *S pneumoniae*	This paper	N/A
PCR primers for PAFR	This paper	N/A
Recombinant DNA		
PAFR-overexpressing plasmid and the control vector	Shanghai GeneChem Co. Ltd	N/A
Software and algorithms		
Dose Calculator software	Siemens Medical Solutions	https://www.siemenshealthineers.com
using GraphPad Prism 7 software	GraphPad Inc	https://www.graphpad.com
IBM SPSS Statistics 20.0 software	IBM Inc	https://www.ibm.com

RESOURCE AVAILABILITY

Lead contact

Further information and requests for resources and reagents should be directed to and will be fulfilled by the lead contact, Feng Jiang (fjiang@som.umaryland.edu).

Materials availability

This study did not generate new unique reagents.

Data and code availability

- All other data generated and analyzed in this study are available within the article and the supplemental information.
- This study did not generate any code.
- Any additional information required to reanalyze the data reported in this paper is available from the lead contact upon reasonable request.

EXPERIMENTAL MODEL AND SUBJECT DETAILS

Bacterial strain and culture conditions

The strains of *SP* (NCTC10319) and *E. faecalis* (BAA-2128) were obtained from National Collection of Type Cultures (NCTC , England, UK) and American Type Culture Collection (ATCC, Manassas, VA), respectively. The bacteria were cultured in medium according to the manufactures' instructions.[14,39] The concentration was adjusted to a density of 5×10^6 colony forming unit (CFU)/mL by suspending bacteria in

phosphate-buffered saline (PBS) (Sigma-Aldrich, St. Louis, MO).[14,33,39] To prepare heat-killed bacteria, bacterial cells were incubated at 95°C for 30 min.[40]

Cell culture

Human NSCLC cell lines (H226, H460, and H1299) and the normal lung cell line (BEAS-2B) were purchased from the ATCC. The cell lines were cultured as described in our previous studies.[14,41–43] WEB2086, a PAFR antagonist, was purchased from Sigma-Aldrich (Sigma-Aldrich).

Clinical specimens

This study was approved by the Institutional Review Board (IRB) of University of Maryland (HP-00040666). Lung tumor tissues and noncancerous lung tissues from 86 consecutive NSCLC patients were obtained from University of Maryland Medical Center. The patients underwent either a lobectomy or a pneumonectomy from 2007 to 2016. The disease-specific survival time was calculated from the date of surgery to death from cancer-related causes. Demographic and clinical characteristics of the patients with lung cancer are shown in Table 1. The histologic tumor type was determined according to World Health Organization classification. Of the NSCLC patients, 74 had AC and 64 had SCC, while 31, 59, and 48 were diagnosed with stage I, II, III, and III-IV, respectively.

METHOD DETAILS

Cell adhesion and invasion assays

Cell adhesion assay was performed as previously described.[6,14,21,33,39] Briefly, cells were seeded onto the wells of 24-well plates at 10^6 cells/well. Bacteria from mid-logarithmic phase (A620, OD = ~0.55) were washed in PBS, resuspended in DMEM supplemented with 10% fetal bovine serum (FBS) (Sigma-Aldrich), and added to the wells at a multiplicity of infection (MOI) of 10. The plates were incubated at 37°C with 5% CO_2 for 90 min and then washed with PBS. To count the number of bacteria, cells were lysed with PBS containing 0.025% Triton X-100 (Sigma-Aldrich). To determine cell invasion, the initial steps were the same as those in the adhesion assay, but that penicillin (100 μg/mL) (Sigma-Aldrich) and gentamicin (50 μg/mL) (Sigma-Aldrich) were added to the culture media. The cells were removed from the wells by using 0.25% trypsin (Sigma-Aldrich) and 0.02% EDTA (Sigma-Aldrich). The cells were lysed by saponin (Sigma-Aldrich), serially diluted, plated on sheep blood agar plates, and incubated under anaerobic conditions for 24 h. Six replicates were performed for each experiment at least three times.

RNAi

Specific siRNAs targeting PARF, PI3K, AKT, and NF-kB were designed as follows: PARF, sense, GGGAUAU CUACUGUGGUCUtt; antisense, AGACCACAGUAGAUAUCCCtt, PI3K, sense, AGTTCCCAGATATGTCA GTuu, antisense, ACTGACATATCTGGGAACTuu, AKT, sense, CUGACCAAGAUGACAGCAU, antisense, AUGCUGUCAUCUUGGUCAG, and NF-kB sense, GGACAUAUGAGACCUUCAAdTdT; antisense 5′ UUGA AGGUCUCAUAUGUCCdTdT. Corresponding scrambled sequences were also designed. The siRNAs were synthesized by Integrated DNA Technologies (IDT, Coralville, IA). Transfection was performed by using Opti-MEM medium and Lipofectamine RNAiMAX (Thermo Fisher Scientific, Allentown, PA) as previously described.[41,43,44]

Construction of mutants

We generated PspC or PsaA -deficient mutants of NCTC 10319 by replacing the sequences with the erythromycin gene cassette as described previously.[45–48] We used PCR to amplify the full-length genes from the chromosomal DNA of NCTC 10319 with the primers (PspC) 5′-GGATCCTTGTTTGCATCAAAAAGC GAAAG-3′ and 5′-AAGCTTGTTTAGTTTACCCATTCACCATTGGC-3′, (PspA) 5′-CGCGGATCCAAGCT TATGATATAGAAATTTGTAAC-3′ and 5′-GAGGAGCTCTTAAACCCATTCACCATTGGC-3′, which incorporated flanking BamHI and HindIII restriction sites. We cloned the amplified DNA into digested pQE30 (Qiagen, Germantown, MD). We deleted a SpeI digest of the inserted fragments (nt 550–1080). The plasmid was blunt-end ligated with and the erythromycin gene cassette. We verified the integrity of the antibiotic gene cassette by sequence analysis using ABI Prism dye terminator cycle sequencing (Thermo Fisher Scientific). Erythromycin (5 μg mL) (Sigma-Aldrich) was added to the growth medium for the mutants. The transformation of pneumococci was carried out as described previously.[45–48]

Ectopic PAFR expression

PAFR-overexpressing plasmid and the control vector expresses sequence that lacks significant homology to the human genome databases were purchased from Shanghai GeneChem Co. Ltd (Shanghai. China). All constructs were confirmed by DNA sequence. Lipofectamine 2000 (Thermo Fisher Scientific) was used for transfection according to the manufacturer's instructions. The transfected cells were selected with G418 (Thermo Fisher Scientific) to generate stable cell lines.

Cell proliferation and migration assays

Cell proliferation was performed as described in our previous studies.[43,44,49] Cell migration was determined by using transwell assay.[43,44,49] The cells that had migrated to the lower surface of the membrane were fixed with formalin and stained with crystal violet (Sigma-Aldrich). The migrating cells were examined microscopically and determined by counting the migrating/invasive cells in 5 randomly selected fields using an Olympus BX41 microscope (Olympus, Waltham, MA).

Immunohistochemistry and Western blotting

We performed immunohistochemistry by using Dako envision dual link system-HRP (DAB+) (Dako, Carpinteria, CA) according to the manufacturer's instructions. To perform Western blot, we used T-PER Tissue Protein Extraction Reagent (Thermo Fisher Scientific) to extract proteins from the cells, which were loaded on to the 10% polyacrylamide sodium dodecyl sulfate gels and then transferred to nitrocellulose membranes. We detected proteins by using enhanced chemiluminescence. Antibodies for immunohistochemistry and Western blotting were purchased from Abcam (Abcam, Cambridge, MA).

PCR array analysis of pro-inflammatory cytokine gene expression

Pro-inflammatory cytokine gene expression was determined in cell or tissue specimens by using a 96 well RT2 Profiler PCR Array for inflammatory cytokines (SABiosciences, Frederick, MD) according to the manufacturer's instructions. Briefly, one μg RNA was used in cDNA synthesis by RT2 first strand kit (SABiosciences). The cDNA was added to a 96-well RT2 Profiler PCR Array for inflammatory cytokines (SABiosciences). A Light Cycler 480 (Roche Diagnostics, Indianapolis, IN) was used for the PCR analysis. Cycle threshold values (CT) were converted into fold change.

Pro-inflammatory cytokines analysis

FirePlex-96 Key Cytokines (Mouse) Immunoassay Panel (ab235656) (Abcam) was used to determine pro-inflammatory cytokines in serum samples according to the manufacturer's manual. Analysis of data was performed by using the Fireplex Analysis Workbench (Abcam).

FISH

FISH was performed as previously described.[50–52] Briefly, Alexa Fluor 594-conjugated specific probe (CACTCTCCCCTCTTGCAC) for *SP* was used for the detection (Thermo Fisher Scientific). Cells were fixed by adding ethanol, from which cytocentrifuge slides were made. Air-dried slides were incubated with a solution of 1 mg/mL lysozyme (Sigma–Aldrich) at 30°C and followed by 1 mg/mL lysostaphin (Sigma–Aldrich). The hybridization buffer included 0.9 M NaCl, 20 mM Tris–HCl (pH 7.3) and 0.01% sodium dodecyl sulphate. Pre-warmed hybridisation solution (20 μL) was mixed with 10 pmol of the oligonucleotide probe and applied to the slides. After incubation 49°C for overnight, slides were rinsed with water and mounted with VECTASHIELD Mounting Medium containing DAPI (Vector Laboratories, Burlingame, CA). The slides were examined and images were taken under microscopes equipped with appropriate filter sets (Leica Microsystems, Buffalo, NY).

Droplet digital PCR (ddPCR) analysis of DNA abundance of SP and mRNA expression of PAFR

Genomic DNA from cell lines and surgical tissue specimens was extracted using QIAamp DNA Kit (QIAGEN). ddPCR was used to detect DNA of *SP* by using a QX100 Droplet Digital PCR System and 2× ddPCR Supermix (Bio-Rad, California, CA) with protocols developed in our previous studies.[53–62] The primers for *SP* were F-5′-GCAGTACAGCAGTTTGTTGGACTGACC and R-5′-GAATATTTTCATTATCAGT CCCAGTC. We used the software provided with the ddPCR system for data acquisition to calculate the concentration of target DNA in copies/μL from the fraction of positive reactions using Poisson distribution analysis. For quantification of PAFR mRNA, total RNA was isolated by QIAGEN RNA preparation kit (QIAGEN). mRNA level of PAFR was determined by using ddPCR with specific primer for the gene

(F-5′-GGTGACTTGGCAGTGCTTTG and R-5′-CACGTTGCACAGGAAGTTGG).[63] Copies/μL of PAFR mRNA was directly determined by using the software of the ddPCR system with Poisson distribution analysis.

Tumorigenicity sssay in nude mice

The animal study was performed with the approval of the University of Maryland under code IACUC# 0516007. Six-week-old male nude mice (BALB/C) were purchased from Charles River Laboratory (Wilmington, MA) and randomly divided into three groups (5 mice per group). Mice in group 1 were injected subcutaneously with 1×10^6 NSCLC cells incubated with 50 μL SP or PBS. Mice in group 2 and 3 were injected with 1×10^6 NSCLC cells only or PBS. All mice were intraperitoneally injected with 150 mg/kg piperacillin (Pfizer, New York, NY) and raised in the specific pathogen−free conditions with autoclaved food and water. The tumor volumes were monitored three times per week using the formula V = (length [mm]) X (width [mm]) 2×0.52.[64] The tumor size was represented by mean ± standard deviation (SD) mm^3. Mice were euthanized on day 28 under deep anesthesia with pentobarbital (Sigma-Aldrich). The tumor weight was measured and then used for downstream molecular analysis.

A tobacco carcinogen–induced mouse lung cancer model

Six-week-old female A/J mice were purchased from the Jackson Laboratory (Bar Harbor, ME) and housed in the specific-pathogen-free animal quarters of Animal Core Facility, University of Maryland. After 1 week of accommodation, mice were randomly divided into four groups (12 mice per group). Mice in group 1 were treated with PBS only. Mice in groups 2, 3 and 4 were treated with two doses of 4-(Methylnitrosamino)-1- (3-Pyridyl)-1-Butanone (NNK) (100 mg/kg, i.p.) at an interval of a week apart. After the second NNK dose, group 3 mice received intranasal instillations of SP (2×10^6 CFU) weekly for 14 weeks. Group 4 mice received intranasal instillations of SP (2×10^6 CFU) weekly and intraperitoneal injection of WEB2086 at 5 mg/kg weekly.[65] To assess lung tumor burden, we euthanized 6 mice with an overdose of CO2, harvested lungs, counted tumors, and measured the sizes at week 24. Serum samples were collected for analysis of inflammatory cytokines. We dissected lung tumors and the surrounding noncancerous lung tissue for downstream molecular analysis. The remaining mice in each group were monitored regularly until spontaneous death occurred.

Micro-CT images of the tobacco carcinogen–induced mouse lung cancer A/J model

Micro-CT images were taken as previously described.[66,67] Briefly, mice were anesthetized, endotracheally intubated, connected to a Flexivent ventilator (Scireq, Montreal, Canada) and administrated isoflurane at 2% concentration until complete relaxation. The mice were then scanned with a Micro-CAT II (Siemens Pre-Clinical Solutions, Knoxville, TN) X-ray micro-CT, with a source voltage of 80 kVp and a current of 500 μA. Seven hundred projections were acquired during 650 ms iso-pressure peak inspiration breath holds, with an exposure time of 450 ms per projection. The average scan time was 32 min, and the dosage was 70.1 cGy per scan as computed by the Dose Calculator software (Siemens Medical Solutions). All images were calibrated to Hounsfield Units using a water phantom. The micro-CT images had 46 μm/pixel isotropic dimensions. The reconstructed 3D images were performed and analyzed by using the Amira 4.1.1 software (Mercury Computer Systems, Inc., Chelmsford, MA) as previously described.[66,68]

QUANTIFICATION AND STATISTICAL ANALYSIS

We determined differences of data between the groups by using one-way ANOVA. Comparisons of means among multiple groups were assessed by 1-way analysis of variance tests. We analyzed the relationships between *SP* abundance and level of PAFR by using linear regression. Spearman correlation analysis was used to determine correlation between *SP* abundance and demographic and clinical characteristics of the patients. We used the median value as cutoff point. The impacts of clinical parameters were estimated by using univariate or multivariate Cox proportional hazards regression model analysis. The Kaplan-Meier survival curves and log rank tests were performed to determine association of *SP* abundance with the disease-specific survival time. The statistical analyses were performed by using GraphPad Prism 7 software (GraphPad Inc. San Diego, CA) and IBM SPSS Statistics 20.0 software (IBM Inc, Armonk, NY).